KeAi

CHINESE ROOTS
GLOBAL IMPACT

Contents lists available at ScienceDirect

Petroleum Science

journal homepage: www.keaipublishing.com/en/journals/petroleum-science



Original Paper

The influence of multi-metal-veins on fractures propagation investigated by the experiment and simulation



Xiao-Dong Hu ^{a, *}, Shao-Bo Han ^a, Shou Ma ^b, Fu-Jian Zhou ^a, Yang Qiu ^a, Xin-Tong Li ^a, Ming-Hui Li ^a, Zhi-Yong Tu ^a

- ^a Unconventional Petroleum Research Institute, China University of Petroleum-Beijing, Beijing, 102249, China
- ^b Sinofts Petroleum Service Ltd, Beijing, 101100, China

ARTICLE INFO

Article history:
Received 26 July 2022
Received in revised form
1 November 2022
Accepted 7 November 2022
Available online 11 November 2022

Edited by Yan-Hua Sun

Keywords:
Multi-metal-veins
Fracture
Fracture interaction
Semi-circle bending test
Numerical simulation

ABSTRACT

Fracture propagation is affected by multi-metal-veins formed by geological diagenesis in shale during the hydraulic fracturing. However, the influence of multi-metal-veins on fractures propagation remains unclear. To solve the problem, based on the semi-circle bending (SCB) test and the extended finite element (XFEM) theory, the interaction between multi-metal-veins and fractures is investigated. The experimental results reveal that the fractures usually deflect at the upper or lower interfaces between metal veins and rocks (e.g. the specimen S-2), which is different from the propagation behavior of fractures in calcite veins. Meanwhile, the fracture toughness of the specimen S-1 is 24.40% higher than that of the specimen S-2, indicating that the increasing of total thickness of multiple metal veins increases the resistance to the fracture vertical propagation. The simulation results show that the increasing of the number, total thickness of veins, the modulus difference between veins and rock, the approach angle and the notch angle all increase the resistance of the fracture passing through metal veins. The maximum deviation distance (D_{max}) of the fracture decreases with the number of veins, while thickness combination types of metal veins do not affect D_{max} . The reduction of the notch angle leads to the more tortuous fracture propagation path. Finally, we propose a new comprehensive fracture network pattern. Fracture networks are divided into two categories, including orthogonal fracture networks and sub-orthogonal fracture networks, and then divided into six sub-categories further. The research results will provide reference for hydraulic fracturing of shale reservoirs containing multi-metal-veins.

© 2022 The Authors. Publishing services by Elsevier B.V. on behalf of KeAi Communications Co. Ltd. This is an open access article under the CC BY-NC-ND license (http://creativecommons.org/licenses/by-nc-nd/4.0/).

1. Introduction

Hydraulic fracturing, as a common practice to enhance the productivity of oil and gas, has been widely used in the development of the shale reservoir in China (Dehghan et al., 2017; Rui et al., 2018; Pan et al., 2019; Guo et al., 2020; He et al., 2020; Li et al., 2021, Li et al., 2022a, b, c). However, due to geological diagenesis, metal minerals (such as pyrite) are relatively developed (Xu et al., 2019; Fan et al., 2021), and a large number of them are distributed in bedding (Yang et al., 2020) in the study area. Multiple metal veins with different thickness and inclination angles are often formed in shale (such as chalcopyrite veins and pyrite veins). This interaction between multi-metal-veins and fractures influences the path of

fracture propagation to varying degrees, and then influences the effect of hydraulic fracturing. Hence, it is critical to investigate the interaction between multi-metal-veins and fractures.

The research about the interaction between fractures and discontinuities was mainly focused on fractures and frictional interface (Renshaw and Pollard, 1995; Gu and Weng, 2010; Jiang et al., 2019). However, most natural fractures are filled with minerals such as chalcopyrite or calcite (Grieser and Bray, 2007; Gale et al., 2007, 2014). Considering the influence of veins on fracture propagation, some experimental research was conducted. Through the experiment of gypsum cement block to study the interaction between fractures and the single cemented natural fractures, it was found that the angle of intersection is the most important factor affecting this interaction (Bahorich et al., 2012). Based on the SCB test, it was found that the fractures tend to cross the single vein easily as the approach angle increases, and the fractures tend to

E-mail address: huxiaodong@cup.edu.cn (X.-D. Hu).

^{*} Corresponding author.

divert into the vein when the approach angle decreases (Wang et al., 2013; Lee et al., 2015). The interaction between fractures and the single vein has been studied by the SCB. The results showed that larger approach angles and thinner veins were more likely to cause fractures to cross the veins, which resulted in complex fractures (Wang W.W. et al., 2018). In previous experiments, only the interaction between a single vein composed of calcite or artificial gypsum and a fracture was studied. The influence of multiple metal veins on fracture propagation has not been considered.

Considering the difficulty to produce vein-contained samples, numerical simulation becomes an important method to investigate rock damage, fracture propagation and the interaction of fractures and veins (Li et al., 2017, 2020; Cong et al., 2021). The interaction between a single vein and a fracture was studied by the threedimensional discrete element method. The results show that the interaction between the vein and the fracture becomes stronger when the strength difference between veins and rock matrix increases (Virgo et al., 2013). Based on the three-dimensional discrete element theory and the SCB model, the interaction between a single vein and a fracture was simulated. When the approach angle and strength of veins decreased, fractures were more likely to turn into the veins (Lee et al., 2016). Based on the coupling model of lattice Boltzmann method and the discrete element method, the interaction between fractures and cemented fractures was studied (Chen et al., 2018). The interaction between a single vein and a fracture was simulated based on the three-dimensional discrete element method and the SCB model. It was found that the fracture was more likely to divert into the vein when the approach angle decreases. And when the differential stress increased, fractures tended to cross the veins (Lee et al., 2018a, b). Numerical simulations from previous studies were mainly considered the interaction of the single vein and fracture, and explained mechanism. However, the influence of multiple metal veins on fracture propagation has not been investigated.

As can be seen from the previous discussion, the effect of multiple metal veins on fracture propagation remains unclear. In this paper, we investigated the interaction between the fracture and multi-metal-veins by the SCB test and numerical simulation

method. First, we quantitatively investigated the interaction between multiple metal veins and fractures through the SCB tests. Second, a two-dimensional SCB numerical model based on the extended finite element method was established. Third, the influence of the number of veins, vein thickness, modulus contrast, approach angle and notch angle on fracture propagation was analyzed. Last, on the basis of previous researchers and combined with the research results of this paper, we proposed a new comprehensive fracture network pattern.

2. Methodology

Fig. 1 depicts the flow chart of studying the interaction between the fracture and the veins in this study. In the paper, the interaction includes the influence of multiple metal veins on fracture propagation path and fracture toughness, as well as various fracture networks generated by the interaction. Firstly, based on the semicircle bending (SCB) test, we calculated the fracture toughness of shale containing metal veins, and observed the propagation behavior after the interaction between fractures and veins. Subsequently, based on the numerical simulation, we established a 2D numerical model of the SCB with veins. Through this model, the influence of factors such as the number and thickness of veins on the interaction between fractures and veins was studied, and the difficulty and behavior of fracture propagation were evaluated according to the numerical results. Finally, based on the previous studies and the simulation results of this paper, we proposed a new comprehensive fracture network pattern to systematically describe the interaction results between fractures and veins.

2.1. Experimental

The SCB test theory developed by Chong and Kuruppu (1984) was applied to the calculation of the fracture toughness of materials (Chong et al., 1987; Lim et al., 1993; 1994; Kuruppu et al., 2014). Based on the previous research, the SCB method has been successfully used in the study of the fracture propagation. Although the SCB test does not consider the effect of fluid when studying

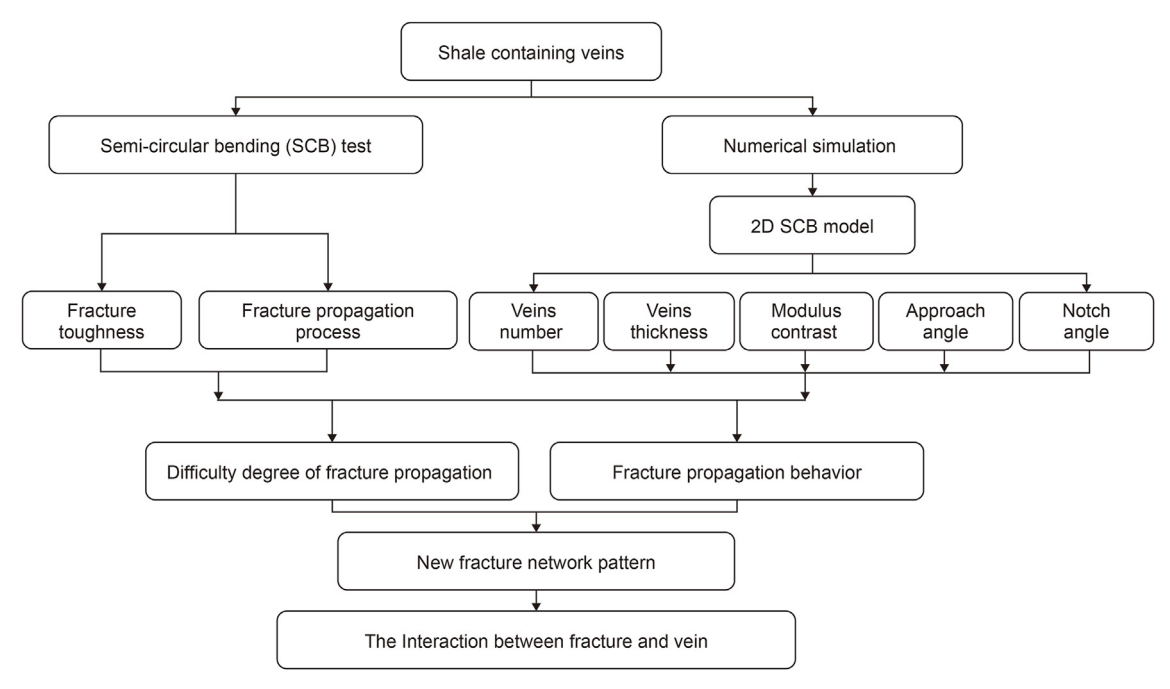


Fig. 1. Flow chart of studying the interaction laws between the fracture and the veins.

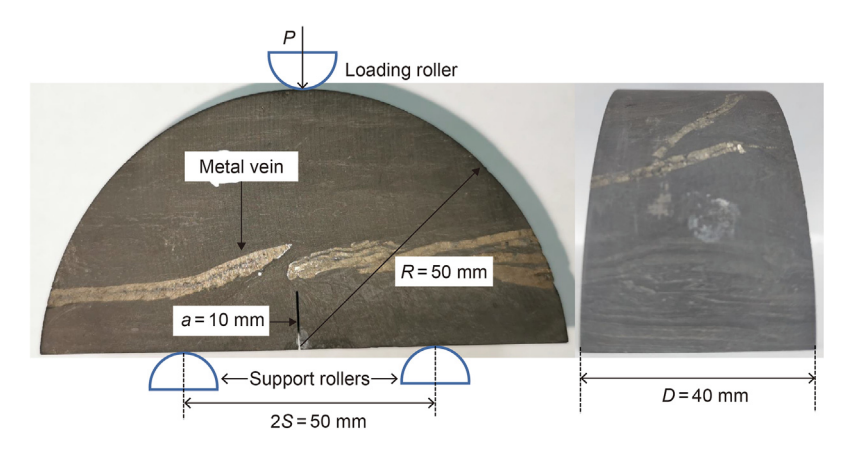


Fig. 2. The geometry size of the SCB shale specimen (*R* is the radius of the specimen; *a* is the length of the notch; *D* is the thickness of the specimen; 2*S* is the distance between support rollers; *P* is the displacement load; the yellow is the metal vein).

Table 1 The specimen parameters.

Radius R, mm	Notch length a, mm	Span 2S, mm	Thickness D, mm	2S/2R	a/R
50	10	50	40	0.5	0.2

fracture propagation, the fracture interactions that occurred in the test were similar to the fluid-driven fractures, and the fractures propagated slowly, which illustrates that the method can be used to investigate hydraulic fractures propagation (Bahorich et al., 2012; Lee et al., 2015; Wang W.W. et al., 2018).

The size of the SCB specimens is consistent with size recommended by ISRM (Kuruppu et al., 2014) (Fig. 2), and the specific parameters of the specimens are shown in Table 1. Through rock mechanics experimental tests, it is found that the average content of metal minerals (pyrite) is about 3%. The load roller was used to apply the displacement load of 0.2 mm/min in this paper. Two support rollers supported the specimens. The acoustic emission sensor was used to receive acoustic emission signals generated by rock fractures (Fig. 3).

2.2. Numerical simulations

Due to the difficulty of producing specimens containing multimetal-veins, it is difficult to obtain sufficient interaction laws between fractures and multiple metal veins through experiments. Numerical simulation has been widely used in the engineering field because of its low experimental cost and fast solution speed. Therefore, the numerical simulation method can be used as another way to study the interaction between multiple metal veins and fractures.

In this paper, a 2D extended finite element (XFEM) model was used to investigate the interaction between multi-metal-veins and fractures. Table 2 shows the mechanics parameters including Young's modulus and Poisson's ratio of rocks, veins and interfaces in the model. Since the samples in this paper were taken from the same area as the samples in the previous study, the parameters in the model were the same as those in the previous publication (Han et al., 2021).

The geometry size of the SCB model shown in Fig. 4 was the same as the size of specimens in the experiment. In Fig. 4, the angle α is the approach angle, which is the angle between the initial fracture direction and the vein. The angle β is the notch angle, which is the angle between the notch and the vertical direction. In fact, metal veins are irregularly distributed in 3D space. If the vein



Fig. 3. Servo hydraulic test system.

with complex shape is considered, the model will be difficult to converge in calculation. Therefore, the current model does not consider the vein in 3D space. For the convenience of research, the irregular metal veins were idealized as rectangles in the model.

The displacement field around the crack tip is discontinuous and infinite during the simulation. To solve the problems above, the extended finite element method (XFEM) introduces two local enhancement functions including the asymptotic function and the step function to approximate the displacement field on the premise of keeping the existing grid. This method uses the asymptotic function $F_{\alpha}(x)$ to capture the singular points near the crack tip. The step function H(x) represents the discontinuous displacement field. The approximate displacement field around fractures is described by Eq. (1) (Stolarska et al., 2001; Fries and Baydoun, 2012; Zeng et al., 2018; Wang B. et al., 2018):

Table 2Material parameters of each part in the model.

Material	Young's modulus E, GPa	Poisson's ratio
Rock Vein	25 50	0.27 0.3
Interface	0.1	0.2

$$\mathbf{u} = \sum_{I=1}^{N} N_I(x) \left[\mathbf{u}_I + H(x) \mathbf{a}_I + \sum_{\alpha=1}^{4} F_{\alpha}(x) \mathbf{b}_I^{\alpha} \right]$$
 (1)

In Eq. (1), the $N_l(x)$ means the shape function; \mathbf{u}_l is the node displacement vector; \mathbf{a}_l is the node enrichment degree of freedom vector; \mathbf{b}_l^{α} is the node enrichment degree of freedom vector at the crack tip.

The discontinuous step function H(x) is given (Wang B. et al., 2018):

$$H(x) = \begin{cases} 1 & \text{if } (\mathbf{x} - \mathbf{x}^*) \cdot \mathbf{n} \ge 0 \\ -1 & \text{otherwise} \end{cases}$$
 (2)

where **x** is a Gaussian point; **x*** is the point on the crack wall pointing to **x**; **n** is the unit where the crack at **x*** is perpendicular to the outside. The asymptotic function $F_{\alpha}(x)$ is given (Lecampion, 2009; Wang B. et al., 2018):

$$[F_{\alpha}(r,\theta),\alpha=1-4] = \begin{cases} \sqrt{r}\sin\left(\frac{\theta}{2}\right) \\ \sqrt{r}\cos\left(\frac{\theta}{2}\right) \\ \sqrt{r}\sin\left(\frac{\theta}{2}\right)\sin\theta \\ \sqrt{r}\cos\left(\frac{\theta}{2}\right)\sin\theta \end{cases}$$
(3)

where (r, θ) is a polar coordinate system whose origin is at the crack tip

The initiation of the fracture is described by the maximum principal stress criterion, as follows:

$$f = \frac{\sigma_{\text{max}}}{\sigma_{\text{max}}^0} \tag{4}$$

where f means the maximum principal stress ratio; σ_{max} and σ_{max}^0 represent the maximum principal stress and the maximum allowable principal stress, MPa, respectively. When f reaches 1, the fracture propagates along the direction perpendicular to the maximum tensile stress.

A 2D SCB model with multi-metal-veins was built (Fig. 5). The model was the ideal model and was only used to illustrate the components of the numerical model. The parameters of the model are shown in Tables 1 and 2. The global seed size of the model was 0.0005. A 4-node bi-quadratic plane strain element (CPE4R) was designated as the element type. The displacement load was 0.2 mm/min. In order to directly observe the fractures propagation path at the interface between the vein and the rock, the interface in the model was replaced with a thin and weak layer (Fig. 5, left).

3. Results and discussion

3.1. Fracture interaction between multi-metal-veins and the fracture in the SCB test

3.1.1. Fracture propagation

A servo hydraulic test system was used to load specimens containing multi-metal-veins, and the fracture propagation path is shown in Fig. 6. The specimen S-1 contains two thick metal veins, the location of which is shown in Fig. 6a. After initiating, the fracture propagates vertically upward into the bottom vein, then crosses the vein and diverts at the upper interface. The fracture propagates a short segment to the left along the upper interface between the metal vein and the rock. Similarly, the fracture crosses the top vein and diverts to the left along the upper interface. Then the fracture propagates in the rock until the specimen completely ruptures. It can be found that the fracture does not divert at the bottom interface between the vein and the rock; at the upper interface, however, the fracture diverts in the same direction. The specimen S-2 contains multiple thin metal veins, the lower two of which are only analyzed, and the position of veins is shown in Fig. 6b. Different from the results of the specimen S-1, the fracture diverts at the upper and lower interfaces of the veins. The

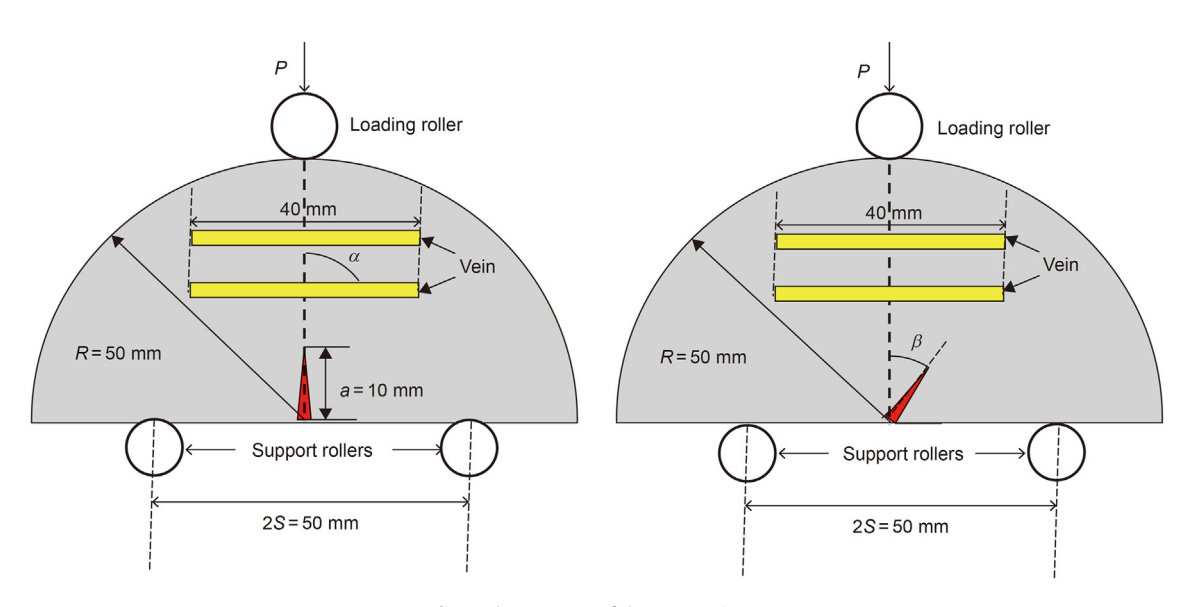


Fig. 4. The geometry of the SCB specimen.

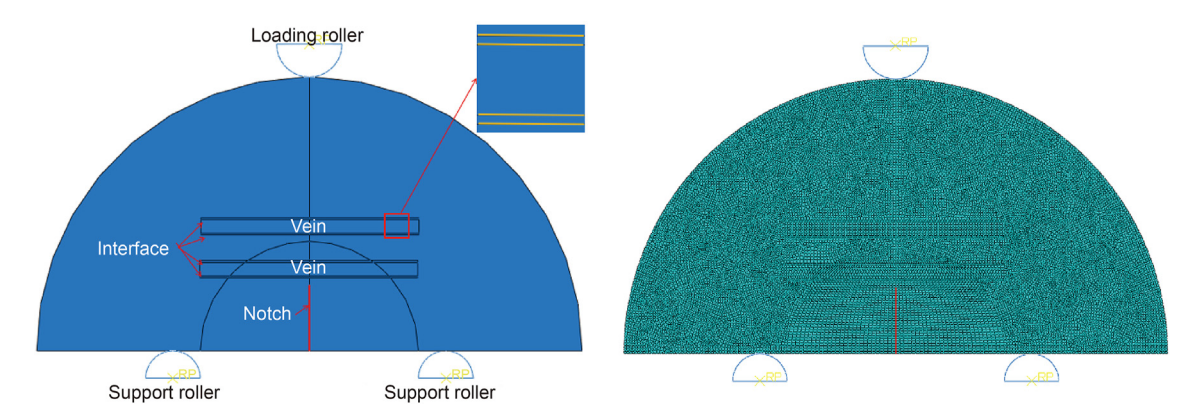


Fig. 5. Model geometry (left) and grid (right).

experimental results indicate that, in specimens S-1 and S-2, the comprehensive influence of multiple interfaces leads to the final fracture propagation pattern.

3.1.2. Fracture toughness

The load-displacement data of the specimens was recorded in the SCB experiment, and the peak load was obtained. Finally, the fracture toughness was calculated by using the peak load and specimens' parameters (Eq. (5) and Eq. (6)) (Kuruppu et al., 2014).

$$K_{\rm IC} = \frac{P_{\rm max}\sqrt{\pi a}}{2RB}Y' \tag{5}$$

$$Y' = -1.297 + 9.516 \left(\frac{2S}{2R}\right) - \left(0.47 + 16.457 \left(\frac{2S}{2R}\right)\right) \chi$$

$$+ \left(1.071 + 34.401 \left(\frac{2S}{2R}\right)\right) \chi^{2}$$
(6)

The specimens containing multi-metal-veins were tested to get the peak load (P_{max}) and fracture toughness (K_{IC}). R is the radius; B is the thickness; a is the notch length; and the value of χ is a/R; A is the dimensionless coefficient. The test results are shown in Table 3.

Fig. 7 shows the load-displacement curves of the specimens containing multi-metal-veins. The peak load of the specimen S-1 is 30.580 kN, and the fracture toughness is 3.320 MPa $\rm m^{1/2}$ (Fig. 7a). The peak load of the specimen S-2 is 23.113 kN, and the fracture toughness is 2.510 MPa $\rm m^{1/2}$ (Fig. 7b). The fracture toughness of the specimen S-1 is 24.40% higher than that of the specimen S-2. The

Table 3Test results for each sample containing multi-metal-veins.

Specimen	P _{max} , kN	K _{IC} , MPa m ^{1/2}
S-1	30.580	3.320
S-2	23.113	2.510

experimental results show that the fracture toughness of the specimens increases as the total thickness of the metal veins increases, which increases the difficulty of the specimens rupturing.

3.1.3. Acoustic emission events and energy of the fractures passing through multi-metal-veins

Acoustic emission (AE) is a phenomenon produced during the fracture of rocks and other materials, which contains important information about the internal failure process of materials. In this paper, the AE is used to analyze the fracture information of shale containing multi-metal-veins.

The curves of acoustic emission (AE) events, energy and load-time in the specimen S-1 are shown in Fig. 8a and b, respectively. The results show that the AE events occur intensively after 100 s, and the number of the AE events is more obvious at 249.58 and 250.16 s. The results of AE energy also show higher energy at these two moments. Two significant fracture events can be inferred at 249.58 and 250.16 s, which are considered to be caused by the fracture passing through the two metal veins. The curves of AE events, energy and load—time in the specimen S-2 are shown in





Fig. 6. Fracture propagation path in SCB test. (a) Specimen S-1; (b) Specimen S-2.

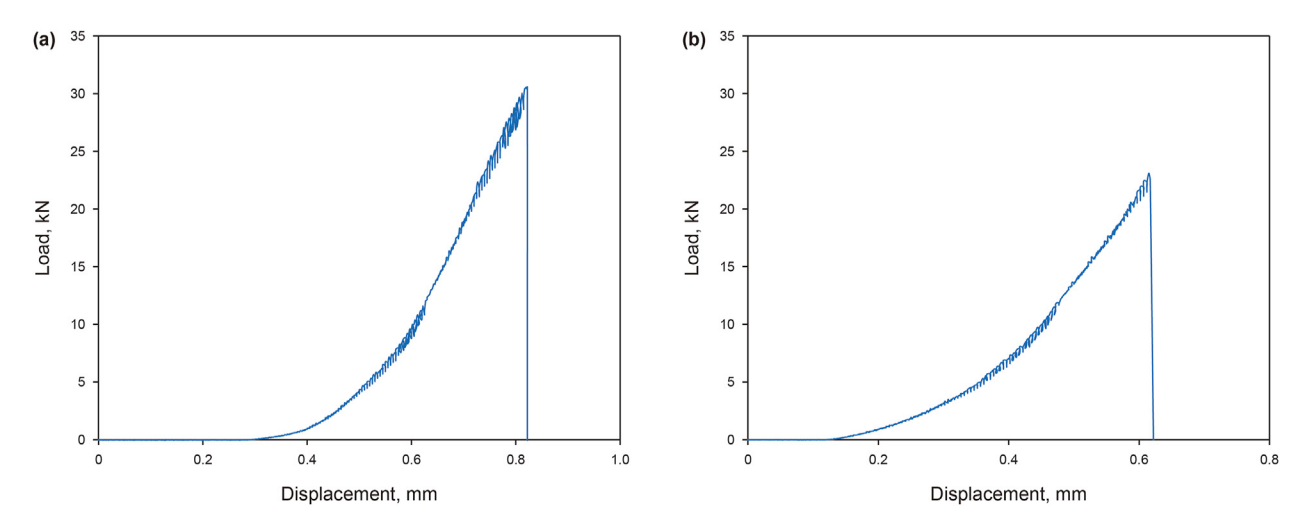


Fig. 7. Load—displacement curves of the samples containing multi-metal-veins. (a) Specimen S-1; (b) Specimen S-2.

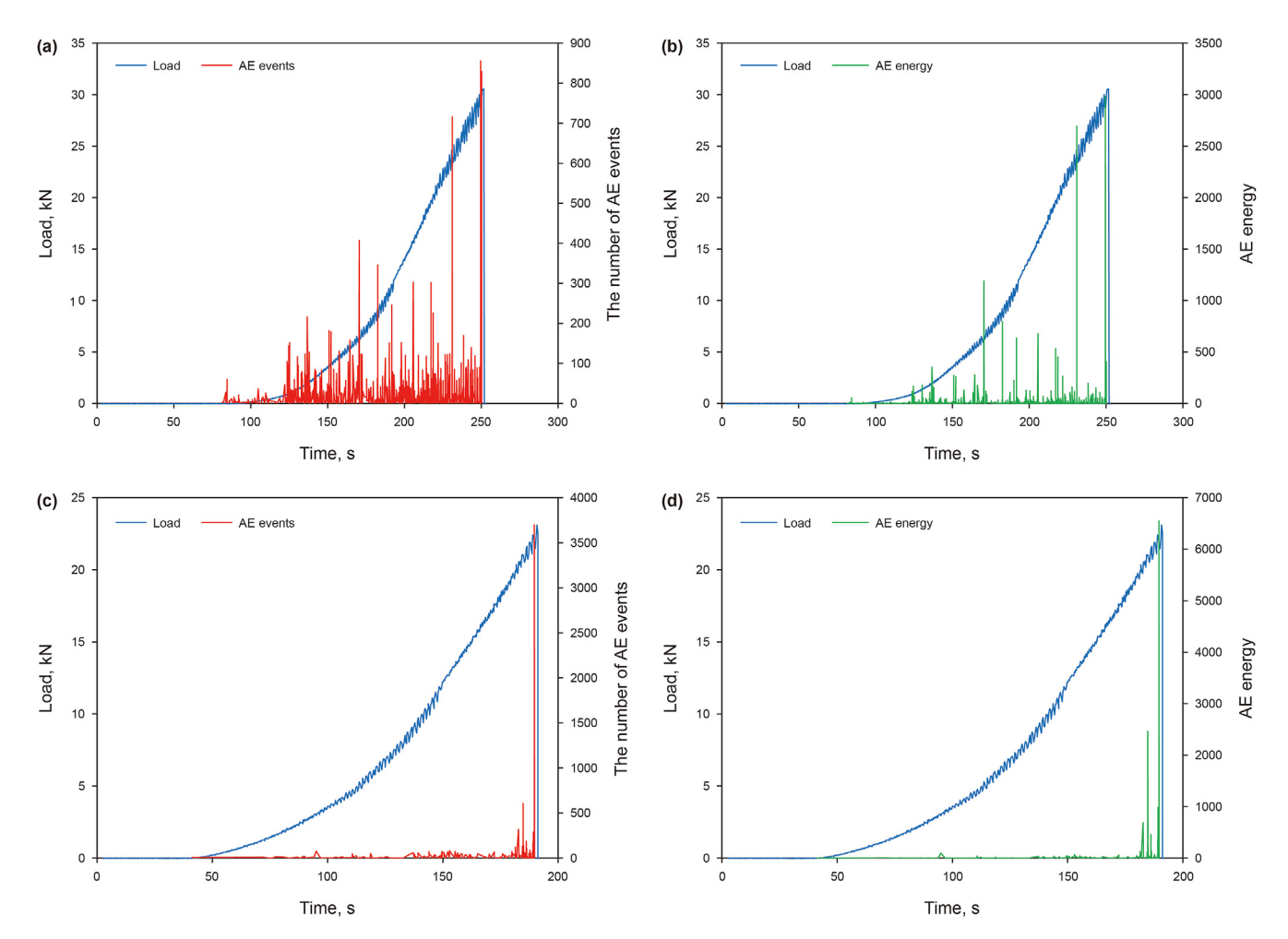


Fig. 8. The number of AE events and AE energy of the samples with multi-metal-veins. (a, b) AE events and load curves, energy and load curves of the specimen S-1, respectively; (c, d) AE events and load curves, energy and load curves of the specimen S-2, respectively.

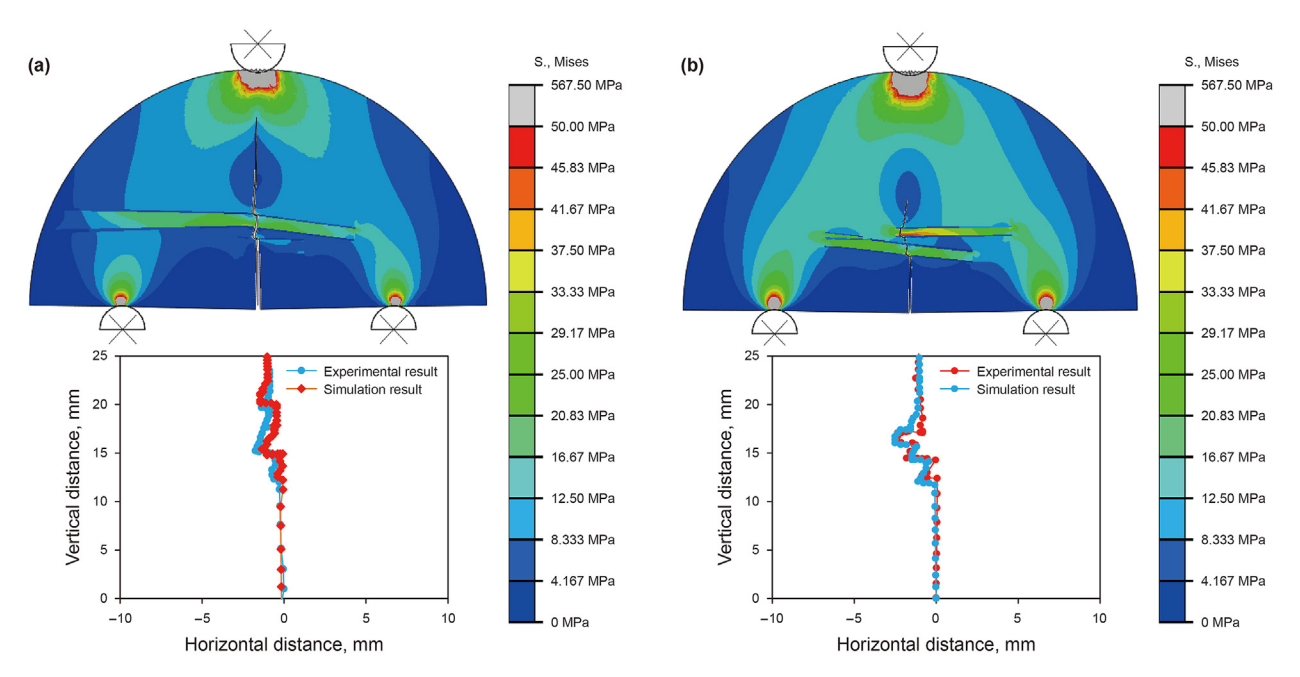


Fig. 9. Comparison of fracture propagation path in SCB test and numerical simulation. (a) Specimen S-1; (b) Specimen S-2.

Fig. 8c and d, respectively. The results show that there are no AE events in the early stage of the whole loading process, and only two maxima appear in 184.81 and 189.64 s in the later stage of loading, which indicates that two fracture events that are considered to be caused by the fracture passing through two metal veins have occurred. The AE experimental results reveal that a strong AE signal is generated when the fracture crosses the metal veins, which can be used to monitor the interaction between the fracture and multiple metal veins.

3.2. Fracture interaction between multi-metal-veins and the fracture in the numerical simulation

We reconstructed the numerical model corresponding to specimens S-1 and S-2 (Fig. 9, top). The simulation results corresponding to specimens S-1 and S-2 (as shown in Fig. 6), and comparison of fracture propagation path in SCB test and numerical simulation are shown in Fig. 9. The results of the numerical simulations were compared with the results of the SCB tests for model

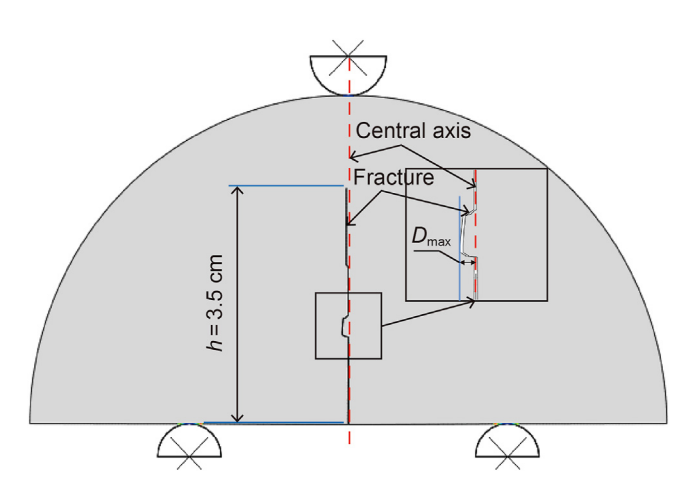


Fig. 10. Schematic diagram of the fracture deviating from the central axis.

validation. The results showed that the fracture propagation paths in the numerical simulation and the SCB test were roughly the same. The errors between the simulation results and the experimental results were about 3.65% (Figs. 9a) and 3.50% (Fig. 9b), respectively.

3.2.1. Fracture propagation path description in the numerical simulation

In order to study the interaction laws between the fractures and the veins, we focused on analyzing the maximum horizontal distance ($D_{\rm max}$) that deviated from the central axis of the specimens when the fracture propagated to a vertical height of 3.5 cm (Fig. 10). At the same time, the time t when the fracture propagates to a vertical height of 3.5 cm was counted. These two parameters were used to describe the characteristics of the fracture propagation.

In all cases, the deflection occurred at the interfaces between the metal veins and the rock before and after the fracture crossed the vein. Now we used the case of the model containing threemetal-veins to illustrate the fracture propagation path. The thickness of the vein is 2.5 mm.

Fig. 11 indicates the Mises stress distribution and fracture propagation path corresponding to different number of veins under the same propagation height condition. The result shows the fracture basically deflects to different degrees when the fracture reaches the upper and lower interfaces between the metal veins and rock (The upper and lower interfaces are the upper and lower surfaces where veins contact rocks). At the same time, the internal stress of the uppermost vein increases as the number of veins increases (Internal stress is the distribution of stress in metal vein). It can be measured that $D_{\rm max}$ is 1.05 mm (1 vein), 0.92 mm (2 veins) and 0.87 mm (3 veins) respectively. The results indicate that $D_{\rm max}$ decreases when the number of veins increases.

A case of 3-veins (Fig. 12) is used to illustrate the fracture propagation process. In Fig. 12a represents the Mises stress contour before and after the fracture crosses the 1st veins. Fig. 12b represents the Mises stress contour before and after the fracture crosses the 2nd veins. Fig. 12c represents the Mises stress contour before and after the fracture crosses the 3rd veins. *t* represents the time for

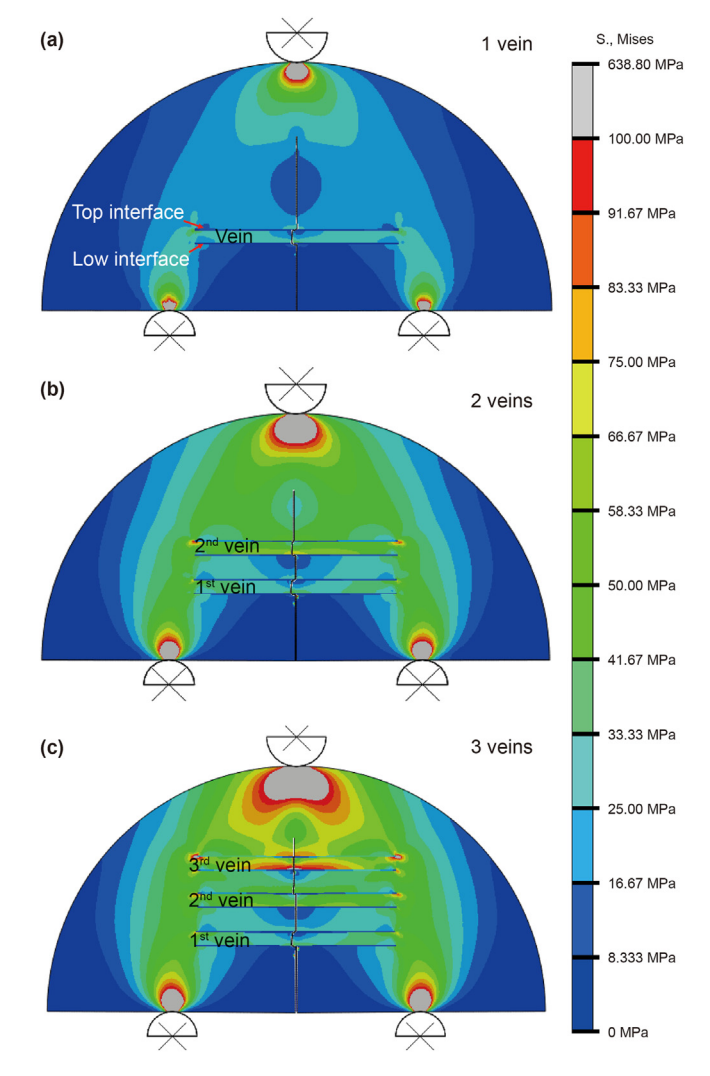


Fig. 11. Stress contours of the models containing different numbers of metal veins: 1 vein, 2 veins, and 3 veins.

the fracture to reach different positions of the vein. The internal stress in the veins becomes higher when the position of the vein becomes higher, which shows that it is more difficult for fractures to pass through veins with the raising of vein position. When the fracture propagates to the first and third veins, a unidirectional high stress zone appears on one side of the crack tip. The fracture diverts at upper and lower interfaces. However, the high-stress areas on both sides of the crack tip are roughly symmetrically distributed before and after crossing through the second vein, and the fracture does not divert. Consequently, the unidirectional high stress is the main factor affecting fracture diversion.

3.2.2. Effect of the number of veins

In order to further analyze the influence of the number of metal veins on fracture propagation, Fig. 13 shows the stress curves of the lower interface of the bottom vein in different models. The positions of the two maximum stresses does not change for different

models in Fig. 13. The result shows that the offset distance of the fracture at the lower interface of the bottom vein is the same (the offset distance at the lower interface of the bottom vein is 1.1 mm).

It can be seen from Fig. 13 that the Mises stress at the lower interface of the bottom vein in the 2-veins model is 1.51% larger than that in the 1-vein model. The Mises stress at the lower interface of the bottom vein in the 3-veins model is 3.51% larger than that in the 1-vein model. The result shows that the stress at the lower interface of the bottom vein increases with the increase of the number of veins, which indicates the resistance to the fracture vertical propagation increases with the increase of the number of veins. In the 3-veins model, the longest time for the fracture to propagate to a height of 3.5 cm is 0.3202 s. The shortest time, however, is 0.2323 s in 1-vein model (Fig. 14). The time when the fracture propagates to a vertical height of 3.5 cm increases by 37.8% as the number of veins increases, which shows that the increasing of the number of veins reduces the speed of vertical fracture propagation.

3.2.3. Effect of thickness of veins

Fig. 15 shows the Mises stress distribution and fracture propagation path corresponding to the combination types of thickness of veins under the same propagation height. Fig. 15a has two 4 mm veins, which is named type-A. Fig. 15b has a 4 and 2.5 mm veins, respectively. The 4 mm-vein located in the upper place, which is named type-B. Fig. 15c also has a 4 and 2.5 mm veins, respectively. The 4 mm-vein located in the lower place, which is named type-C.

The combination types are different, but Mises stress distributions are similar. With different combination types of the veins, $D_{\rm max}$ is 0.90 mm (type-A), 0.95 mm (type-B), and 1.00 mm (type-C), respectively. The result indicates that $D_{\rm max}$ remains basically unchanged when the total thickness of the combination type increases.

In order to illustrate the influence of the combination types on fracture propagation, Fig. 16a and b shows the stress curves at the lower interface of the upper and bottom veins under the different combination types. For the upper veins, the stress around the crack tip at the lower interface of type-B and type-C is roughly the same. The stress around the crack tip of type-A, however, is 30% larger than the first two types. For the bottom veins, the stress around the crack tip of three types is roughly the same. The above results show that the increase of the total thickness of the veins will increase the resistance of the fracture vertical propagation. This conclusion is consistent with the conclusion of the experiment in Section 3.1. However, the position of the maximum stress in the three combination types does not change, which indicates that different thickness combination types do not affect the offset of fractures at the interface. The time when the fracture propagates to a vertical height of 3.5 cm in three types is roughly the same (type-A, 0.2821 s; type-B, 0.2841 s; type-C, 0.2822 s) (Fig. 17), which shows that the thickness combination types of veins hardly affects the speed of vertical fractures propagation.

3.2.4. Effect of modulus contrast

Fig. 18 shows the results of different modulus contrast $(0.5E_{\rm rock}, E_{\rm rock}, and 2E_{\rm rock})$. The thickness of the vein is 2.5 mm. In Fig. 18a–c, the modulus of the veins is $0.5E_{\rm rock}$, $E_{\rm rock}$ and $2E_{\rm rock}$, respectively. The results show that the combination types are different, but Mises stress distributions are similar. With different modulus

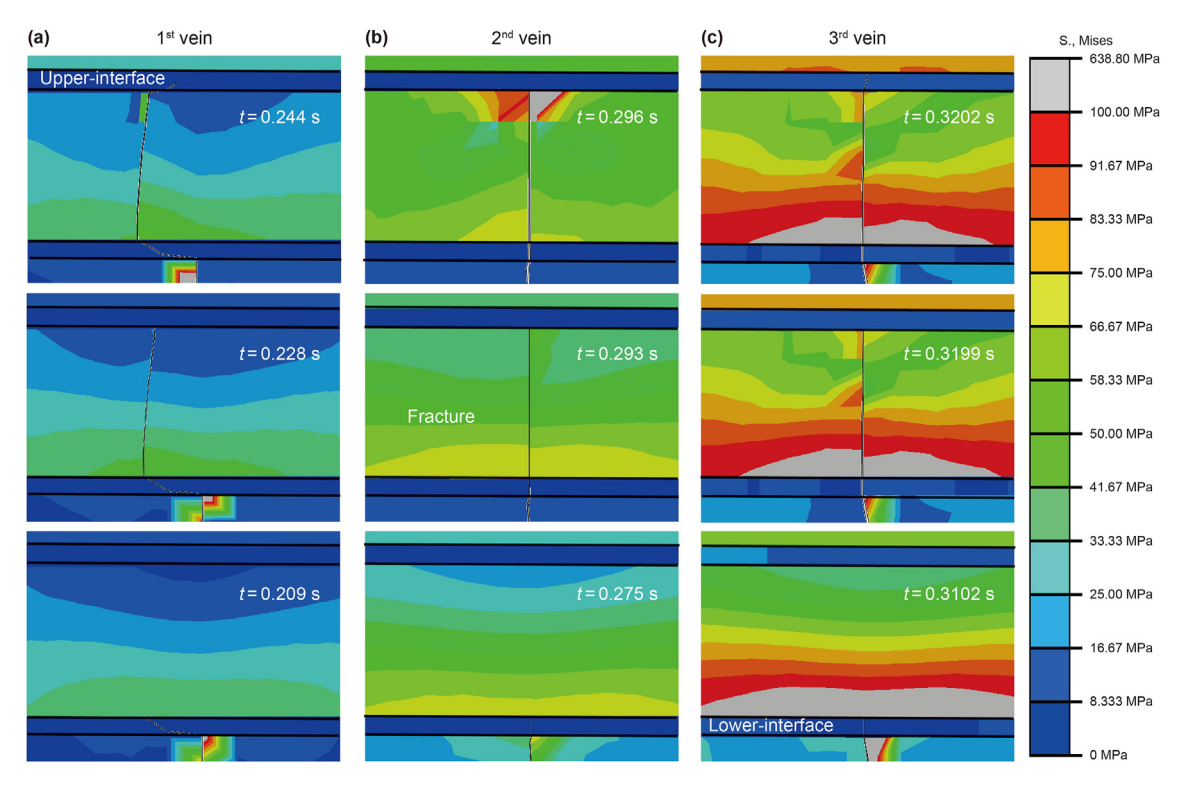


Fig. 12. Stress contours when the fracture propagates in the 3-veins model at different times.

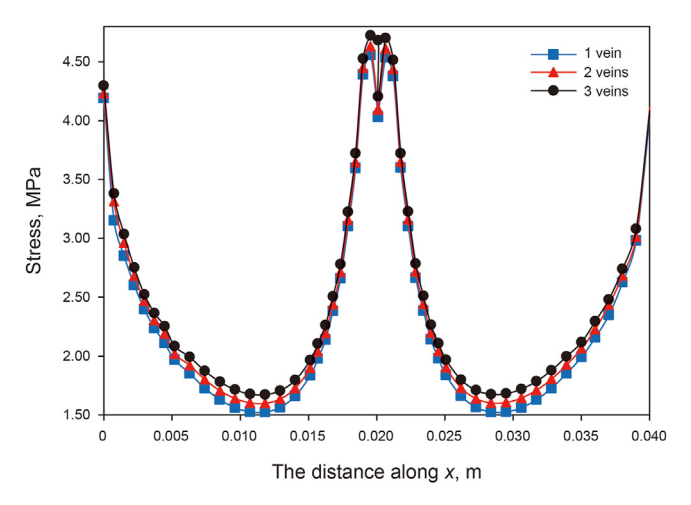
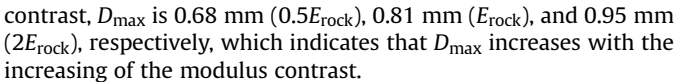


Fig. 13. Comparison of stress curves at the lower interface between the bottom veins and rocks.



In order to further illustrate the influence of the modulus contrast on the fracture propagation, Fig. 19a and b shows the stress curves at the lower interface of the upper and bottom veins under different modulus contrast. For the upper veins, the maximum Mises stress at the lower interface of the upper vein of E_{rock} is 93.2%

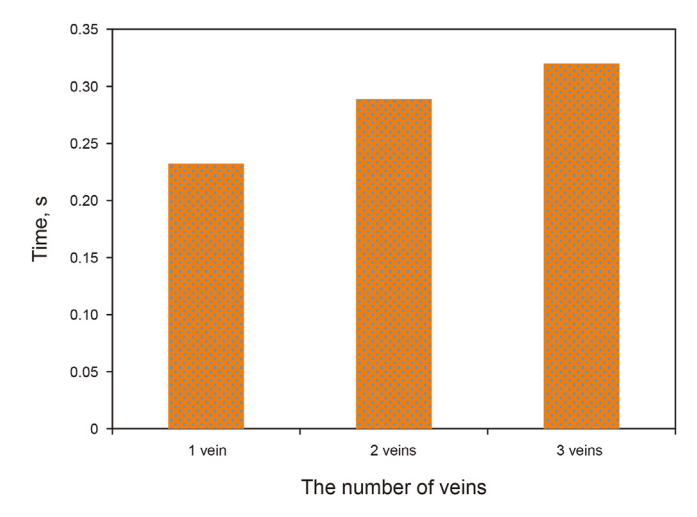


Fig. 14. Time for fracture propagation to a vertical height of $3.5~{\rm cm}$ (1 vein, 2 veins, 3 veins).

higher than that of $0.5E_{\rm rock}$. The maximum Mises stress at the lower interface of the upper vein of $2E_{\rm rock}$ is 79.1% higher than that of $E_{\rm rock}$. For the bottom veins, the maximum value of Mises stress at the lower interface of the bottom vein at $E_{\rm rock}$ is 63.7% higher than that of $0.5E_{\rm rock}$. The maximum value of Mises stress at the lower interface of the bottom vein with a modulus of $2E_{\rm rock}$ is 53.9% higher than that of $E_{\rm rock}$. With the increasing of modulus contrast, the maximum Mises stress of upper and bottom vein increases

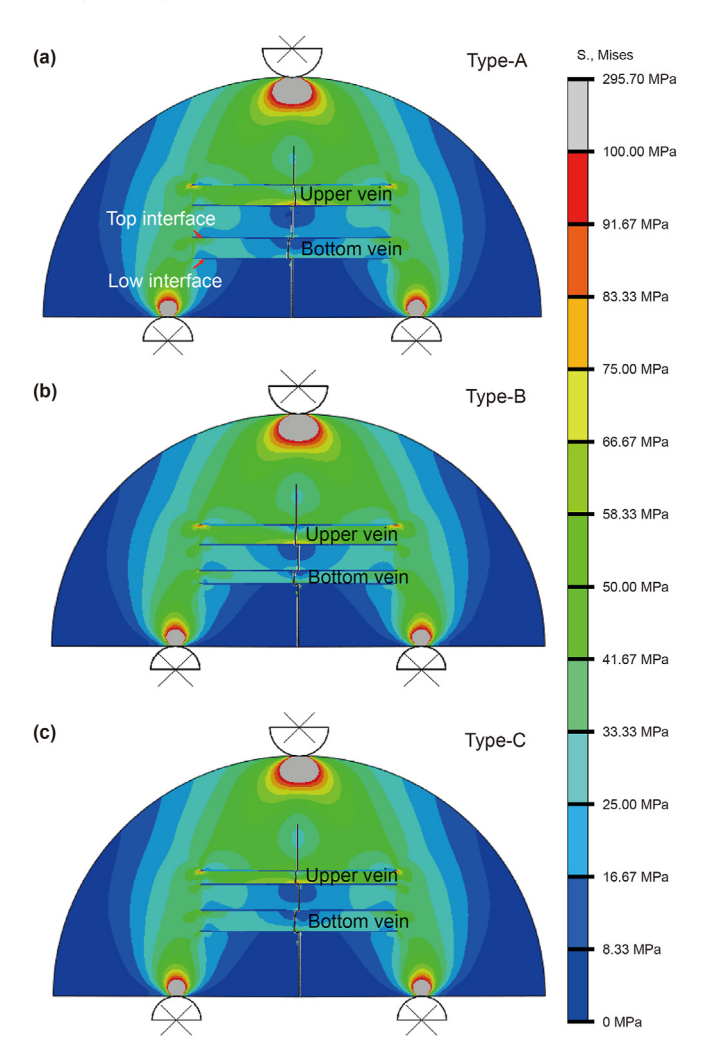


Fig. 15. Stress contours of the models with the different combination types of thickness of veins: type-A, type-B, type-C.

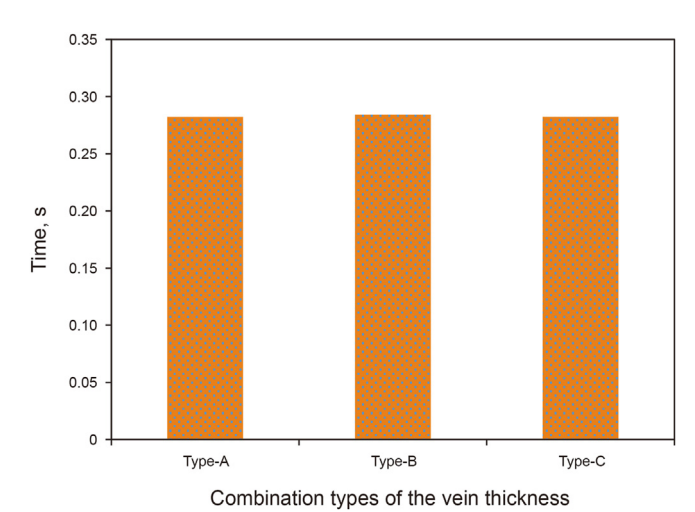
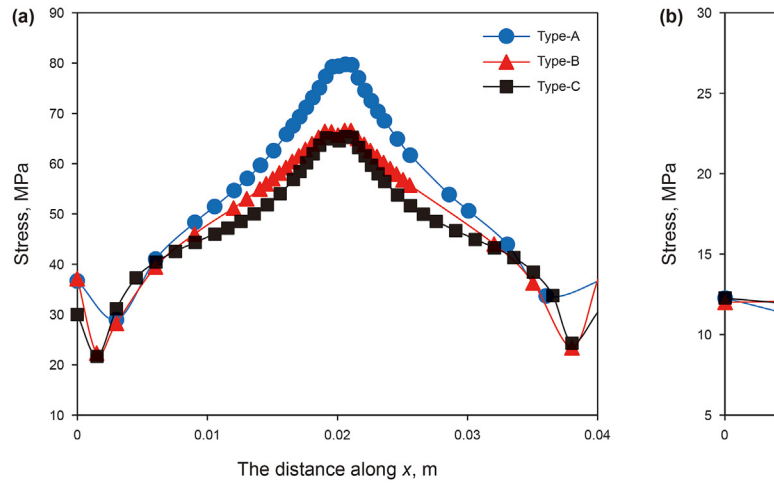


Fig. 17. Time for fracture propagation to a vertical height of 3.5 cm (type-A, type-B, type-C).

greatly. However, the maximum Mises stress of the upper vein increases more. The results show that the difficulty of fracture propagation when the fracture crosses the upper and lower veins increases significantly as the modulus contrast increases. Meanwhile, in the $2E_{\rm rock}$ model, the longest time for the fracture to propagate to a height of 3.5 cm is 0.2888 s. The shortest time, however, is 0.2710 s in $0.5E_{\rm rock}$ model (Fig. 20). The time when the fracture propagates to a vertical height of 3.5 cm increases by 6.57% as the modulus contrast increases, which shows that the speed of vertical fracture propagation is slightly affected by modulus contrast.

3.2.5. Effect of approach angle

The approach angle (α) is the angle between the initial fracture direction and the metal veins. Fig. 21 shows the results of simulation with different approach angles (Figs. 21a and 30°; Figs. 21b and 60°; Figs. 21c and 90°). The thickness of the vein is 2.5 mm. The



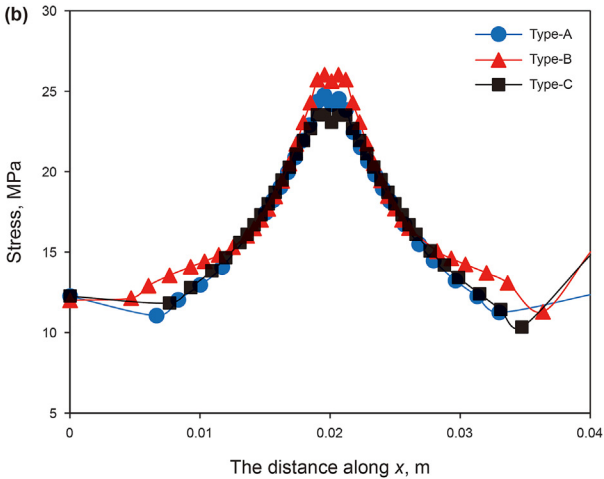


Fig. 16. Stress curves at the lower interface of the upper and lower veins under the different combination types. (a) Upper vein; (b) Bottom vein.

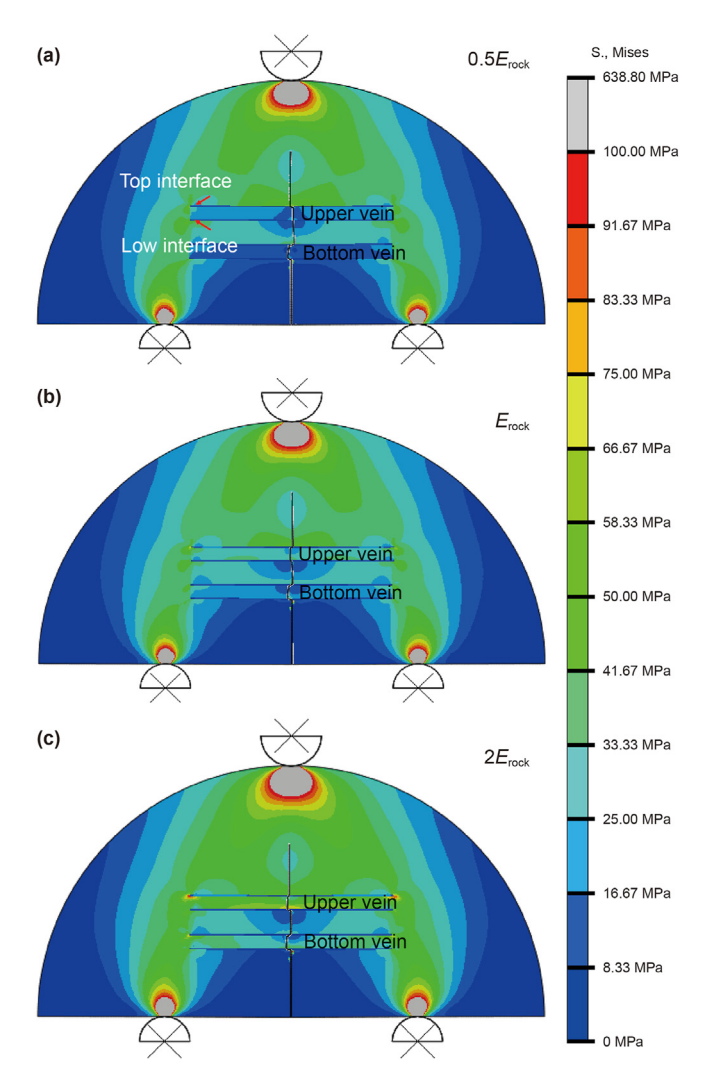


Fig. 18. Stress contours of the models with various vein moduli: $0.5E_{\rm rock}$, $E_{\rm rock}$, and $2E_{\rm rock}$.

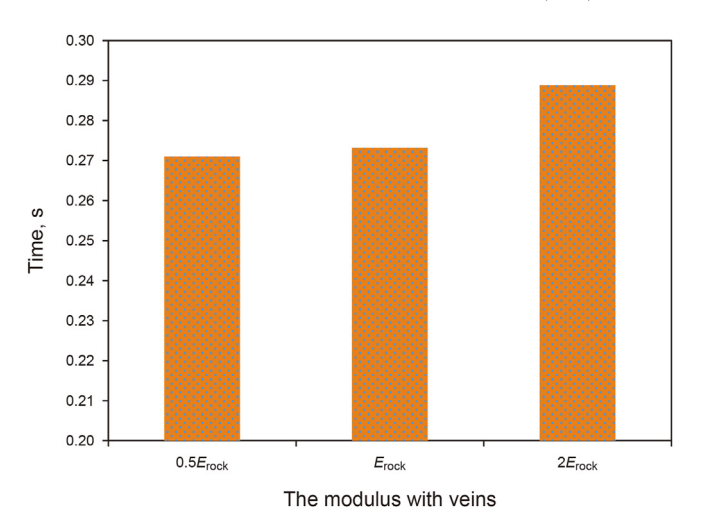


Fig. 20. Time for fracture propagation to a vertical height of 3.5 cm (0.5 $E_{\rm rock}$, $E_{\rm rock}$, and $2E_{\rm rock}$).

results show the Mises stress distributions are different with different approach angles. When the approach angle is 90° , the Mises stress is the largest. So the fracture is difficult to propagate. With different approach angles, $D_{\rm max}$ is $2.04~{\rm mm}~(\alpha=30^{\circ})$, $1.00~{\rm mm}~(\alpha=60^{\circ})$, and $0.92~{\rm mm}~(\alpha=90^{\circ})$, respectively. Therefore, $D_{\rm max}$ decreases with the increasing of the approach angle.

Fig. 22 shows the stress contour of the upper and bottom veins at different approach angles. The results show that the stress at the same position and the resistance to vertical fracture propagation increases as the approach angle increases. In addition, in the 90° model, the longest time for the fracture to propagate to a height of 3.5 cm is 0.2888 s. The shortest time, however, is 0.1961 s in the 30° model (Fig. 23). The time when the fracture propagates to a vertical height of 3.5 cm increases by 47.3% with the increase of the approach angle, which shows that the large approach angle severely reduces the speed of vertical fracture propagation.

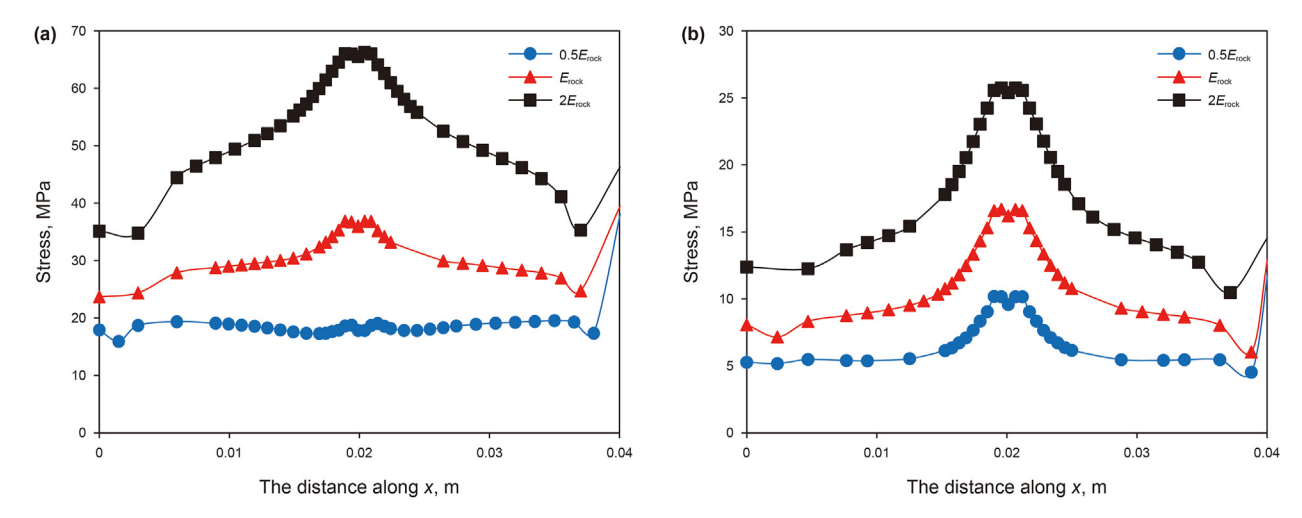


Fig. 19. Stress curves at the lower interface of the upper and lower veins under different modulus contrast. (a) Upper vein; (b) Bottom vein.

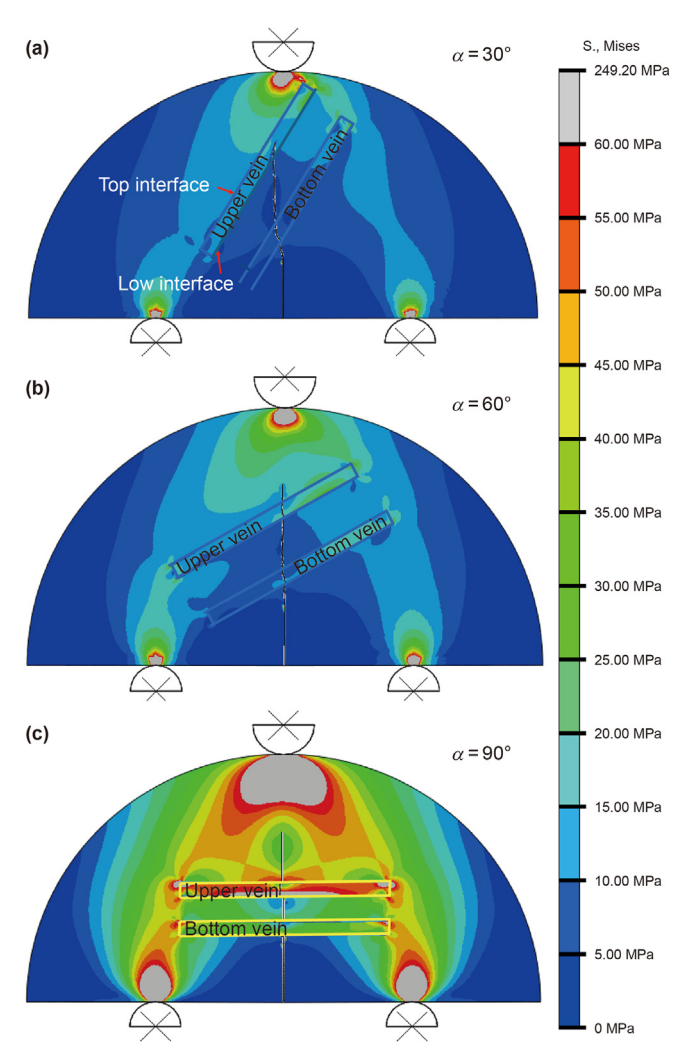


Fig. 21. Stress contours of the models with various approach angles: 30°, 60°, and 90°.

3.2.6. Effect of notch angle

The notch angle (β) is the angle between the initial fracture direction and the vertical direction. Fig. 24 shows the simulation results with different notch angles (30° in Fig. 24a; 45° in Fig. 24b; 60° in Fig. 24c). The thickness of the vein is 2.5 mm. The results show that the Mises stress distributions are different with different notch angles. The Mises stress shows larger values when the approach angle is 60°, so the fracture is difficult to propagate. In addition, the fracture propagation path becomes more tortuous as the notch angle decreases.

Fig. 25 shows the stress curves at the lower interface of the upper and bottom veins under different notch angles. For the upper vein, the stress at the lower interface of the 30° and 45° models is roughly the same. The stress at the lower interface of the 60° model, however, is 150% larger than that of the first two models. For the bottom veins, the Mises stress at the lower interface increases with the increasing of the notch angle. At the same time, it is found that the position of maximum stress at the lower interface of the bottom vein shifts to the right with the increase of the notch angle

(dotted green arrow), which indicates that the position where the fracture crosses the bottom vein is farther away from the central axis of the sample as the notch angle increases. In the $\beta=60^\circ$ model, the time for the fracture to propagate to a height of 3.5 cm is longer than that of the other two models, which is 0.3640 s (Fig. 26).

3.3. Discussion

3.3.1. Fracture network pattern

A simplified diagram of the fracture propagation path in the simulation results is given in Fig. 27. The black solid line represents the fracture propagation path, and the blue dashed line is the central axis of the model. (a) The fracture and multiple metal veins are orthogonal, and the fracture steps in a direction. The number of metal veins does not affect the pattern of fracture network. (b) The fracture and multiple metal veins are sub-orthogonal when the approach angles are 30° and 60°. The fracture and multiple metal veins are orthogonal when the approach angle is 90°. The decreasing of the approach angle makes the fracture deviate further from the initiation direction. (c) The fractures in type-A are orthogonal to the metal veins and step in two different directions. Different from type-A, the fractures in type-B and type-C step in one direction. When the veins are thicker, the fracture tends to step in both directions. (d) When the modulus of the veins is less than or equal to the modulus of the rock, the fractures are more inclined to step in two different directions. When the modulus of veins is larger than that of rock, the fractures tend to step in one direction. (e) When the notch angle is between 0 and 90°, the fractures are sub-orthogonal to the metal veins.

Fracture arrays are defined as one or more pairs of propagating fractures and pre-existing veins. In addition, the fracture network is used as the pattern of the fracture array (Kolawole and Ispas, 2019). In this paper, based on the fracture network classification of Kolawole and Ispas (2019) and the results of this research, we proposed a new comprehensive fracture network pattern. The fracture network is divided into two categories: orthogonal and sub-orthogonal fracture networks. The orthogonal fracture network is further divided into three types: orthogonal, orthogonal-unidirectional stepping and orthogonal bi-directional stepping networks (Fig. 28a). The sub-orthogonal fracture network is further divide into three types: sub-orthogonal, suborthogonal-unidirectional stepping and sub-orthogonal bi-directional stepping network (Fig. 28b). That is, two categories and six sub-categories. The orthogonal network is a type of fracture network generated by the interaction of fractures and veins when the approach angle is 90°. At the same time, in this type, the interaction between fractures and veins is mainly crossing. One of the characteristics of the sub-orthogonal network is that the approach angle is less than 90°, and the interaction between the fracture and the veins is mainly non-crossing (such as diversion and jogging) when the fracture interacts with the vein.

Based on the new fracture network pattern, it can be seen that the interaction between fractures and veins mainly forms an orthogonal-unidirectional stepping fracture network in the simulation results of the number of veins. The small approach angle makes it easier to form sub-orthogonal-unidirectional stepping fracture network between fractures and veins. When the veins are thicker, it is easier to form an orthogonal unidirectional stepping

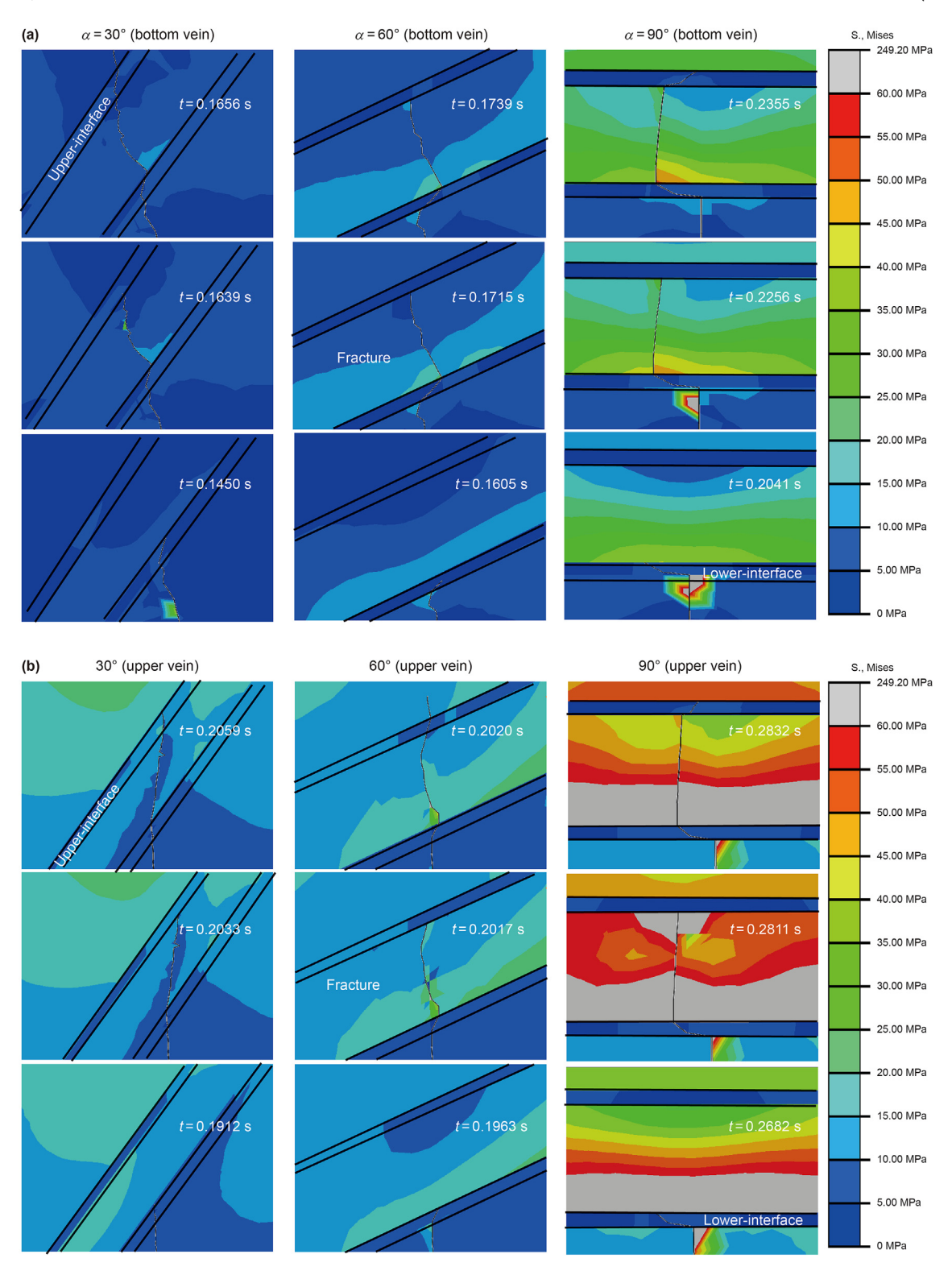


Fig. 22. Stress contours of the models with various approach angles: 30°, 60°, and 90°. (a) Bottom vein; (b) Upper vein.

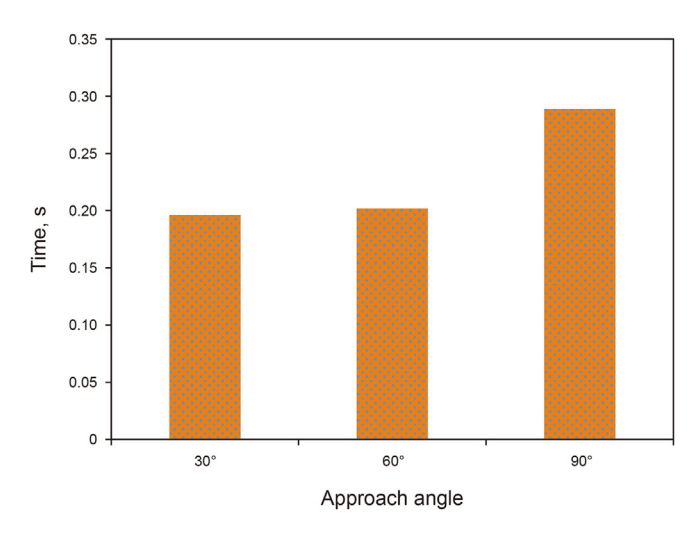


Fig. 23. Time for fracture propagation to a vertical height of 3.5 cm (30°, 60°, and 90°).

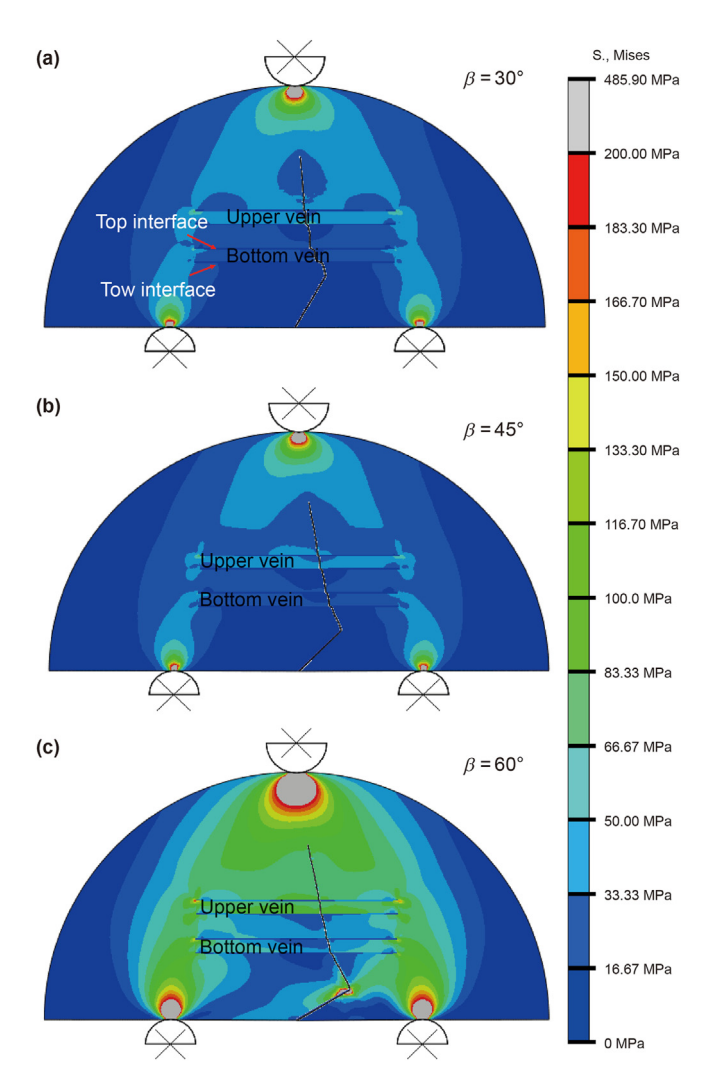


Fig. 24. Stress contours of the models with various notch angles: 30° , 45° , and 60° .

fracture network between the fractures and the veins. When the modulus of the vein is greater than that of the rock, a unidirectional stepping network is more likely to form between the fracture and veins. When the notch angle is between 0 and 90° , the fracture and metal veins always form sub-orthogonal fracture network.

3.3.2. The influence of veins type

The type of minerals has a significant impact on the interaction between the fracture and veins. We take calcite-filled natural fractures as an example to illustrate its influence on the interaction between the fracture and the vein. Based on the SCB test and microscopic test, the interaction between the fracture and calcite veins is investigated (Lee et al., 2015). It is found that the fracture always extends or propagates within the calcite veins when the fracture and veins interact and divert, rather than at the interface between the calcite vein and rock, which may be due to the defects of calcite itself (Fig. 29a) (such as cleavage planes, and fluid or solid inclusions, etc.). In contrast, the fracture is always deflected along the interface between the metal veins and the rock (Fig. 29b). These characteristics eventually lead to the formation of the fracture network patterns described above.

4. Conclusions

Based on the SCB test and XFEM, this study analyzes the interaction between multi-metal-veins and fractures. The following conclusions are drawn through the experiments and numerical simulation:

- (1) In the shale with thin metal veins, the fractures deflected at the upper and lower interfaces between the metal veins and the rock. In shale with thick veins, however, the fractures are not deflected at the lower interface between the metal veins and the rock. The comprehensive influence of multiple interfaces leads to the final fracture propagation patterns. The fracture toughness of the specimens increases with the increasing of the total thickness of the veins. A strong AE signal is generated when the fracture crosses the metal veins, which can be used to monitoring the interaction between the fracture and multiple metal veins.
- (2) The maximum deviation distance ($D_{\rm max}$) of the fracture decreases with the increasing of the number of veins; however, the resistance to the vertical propagation of the fracture increases with the increase of the number of veins. The combination patterns of thickness of veins does not affect $D_{\rm max}$, but the increasing of total thickness of veins will increase the resistance to fracture vertical propagation.
- (3) The $D_{\rm max}$ and the resistance of vertical fracture propagation will increase with the increasing of the modulus contrast. The $D_{\rm max}$ will decrease when the approach angle increases, but the resistance of fracture propagation will increase with the increasing of the approach angle. The reduction of the notch angle results in a more tortuous fracture propagation path, and the position where the fracture crosses the bottom vein is close to the central axis of the specimen.
- (4) In this paper, a new comprehensive fracture network patterns is proposed. In this pattern, fracture networks are divided into two categories: orthogonal fracture networks and sub-orthogonal fault networks, and then into six subcategories including orthogonal, orthogonal-unidirectional

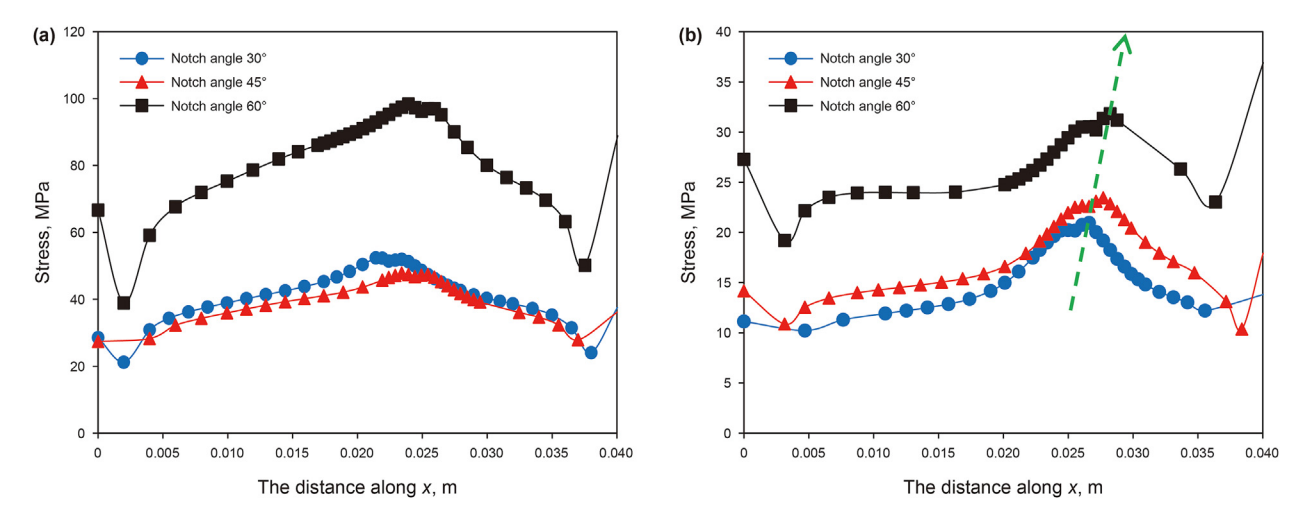


Fig. 25. Stress curves at the lower interface of the upper and lower veins under different notch angles. (a) Upper vein; (b) Bottom vein.

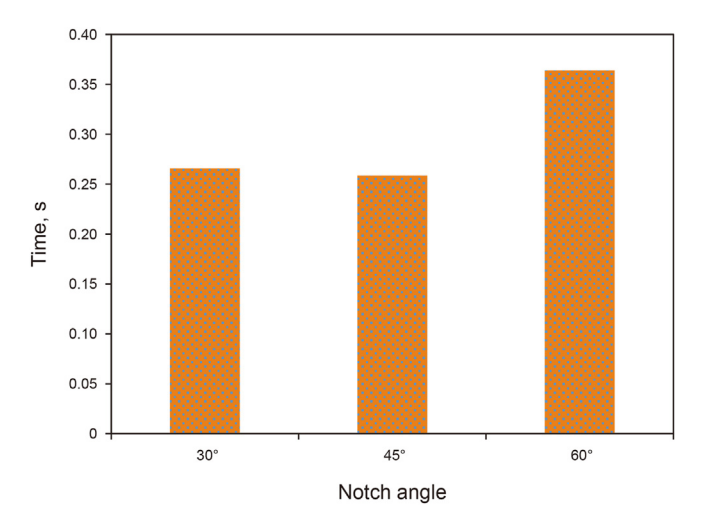


Fig. 26. Time for fracture propagation to a vertical height of 3.5 cm (30°, 45°, and 60°).

- stepping, orthogonal bi-directional stepping, sub-orthogonal, sub-orthogonal-unidirectional stepping and sub-orthogonal bi-directional stepping network.
- (5) Based on the above discussion, the number of veins, total thickness, modulus ratio, approach angle, notch angle, etc. affect the propagation of fractures in shale hydraulic. When the number of veins, the total thickness, the modulus ratio, and the approach angle are larger, the resistance to the vertical propagation of hydraulic fractures is larger. And due to the influence of veins, the path of fractures propagation is also more complicated, among which the initiation direction of hydraulic fractures has the greatest influence. When the angle between the fracture initiation direction and the vertical direction (notch angle) is smaller, the path of fractures propagation is more tortuous. Therefore, in the fracturing process of shale containing metal veins, the influence of metal veins on hydraulic fractures should be fully considered.

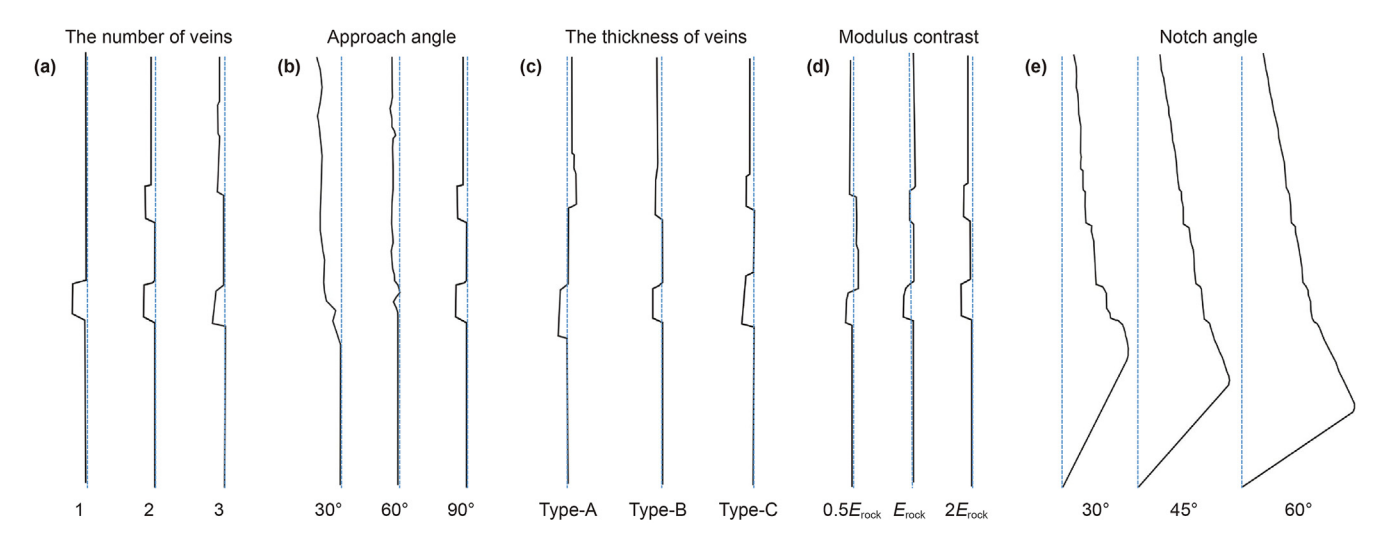


Fig. 27. Simulation results of fracture propagation path (blue dotted line is the central axis of the model; black solid line is the fracture propagation path).

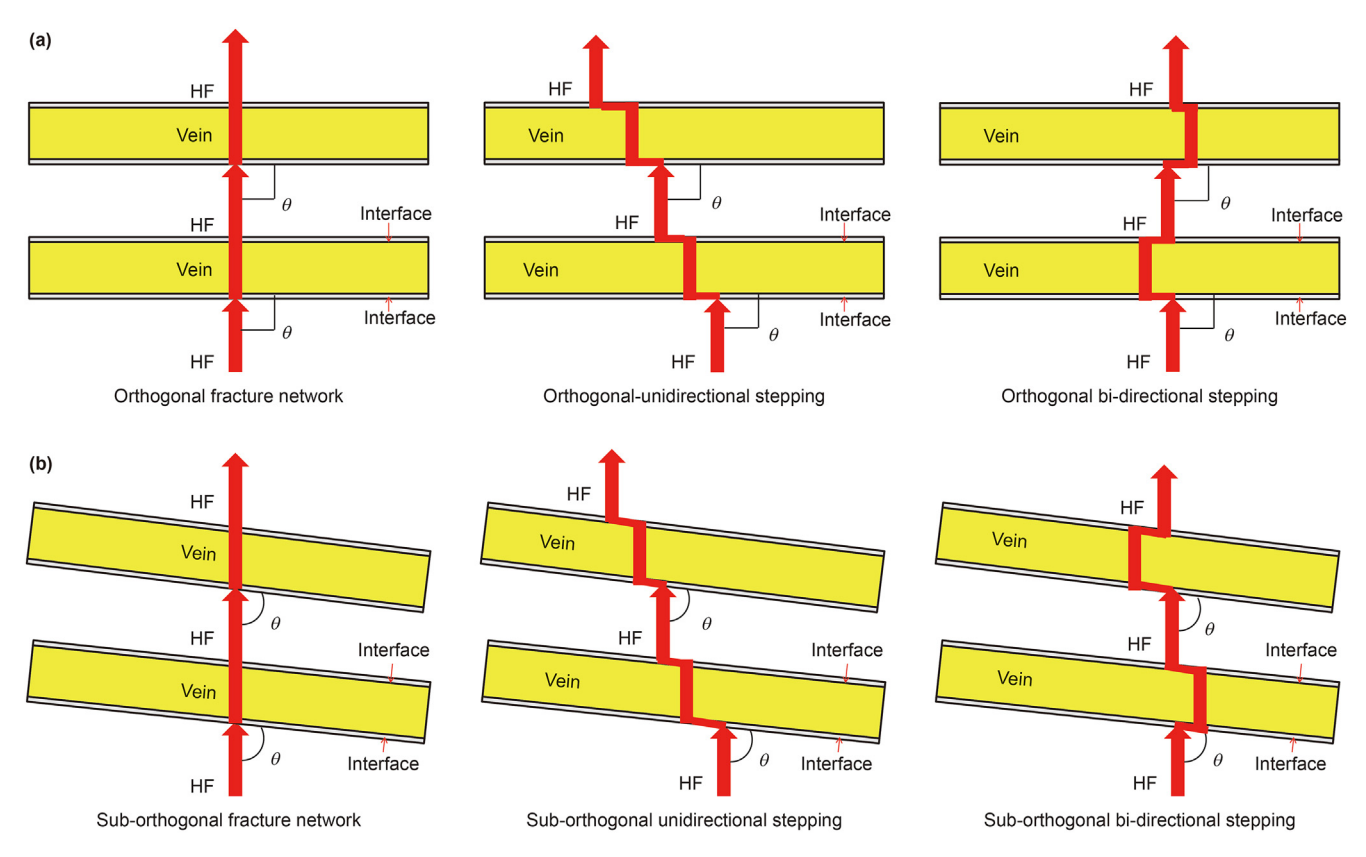


Fig. 28. Fracture network types (array length is 2).

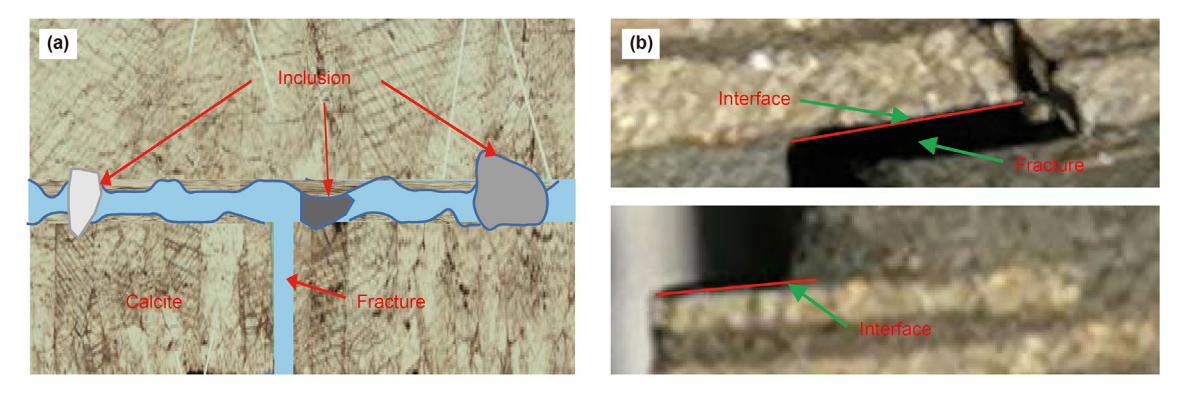


Fig. 29. The path of fractures in calcite and metal veins, respectively. (a) The path of fractures in calcite veins (Lee et al., 2015); (b) The path of fractures in metal veins.

Declaration of competing interest

We declare that we have no financial and personal relationships with other people or organizations that can inappropriately influence our work, there is no professional or other personal interest of any nature or kind in any product, service and/or company that could be construed as influencing the position presented in, or the review of, the manuscript entitled, "The influence of multi-metal-veins on fractures propagation investigated by the experiment and simulation".

Acknowledgement

The authors would like to acknowledge the financial support from the China University of Petroleum (Beijing) School for Young Talent Startup Fund (No. ZX20190183).

References

Bahorich, B., Olson, J.E., Holder, J., 2012. Examining the effect of cemented natural fractures on hydraulic fracture propagation in hydrostone block experiments. In: SPE Annual Technical Conference and Exhibition. Society of Petroleum Engineers. https://doi.org/10.2118/160197-MS.

Chen, Z.Q., Yang, Z.M., Wang, M.R., 2018. Hydro-mechanical coupled mechanisms of hydraulic fracture propagation in rocks with cemented natural fractures. J. Petrol. Sci. Eng. 163, 421–434. https://doi.org/10.1016/j.petrol.2017.12.092.

Chong, K.P., Kuruppu, M.D., Kuszmaul, J.S., 1987. Fracture toughness determination of layered materials. Eng. Fract. Mech. 28 (1), 43–54. https://doi.org/10.1016/ 0013-7944(87)90118-4.

Chong, K.P., Kuruppu, M.D., 1984. New specimen for fracture toughness determination for rock and other materials. Int. J. Fract. 26 (2), R59–R62. https://doi.org/10.1007/bf01157555.

Cong, Z.Y., Li, Y.W., Pan, Y.S., Liu, B., Shi, Y., Wei, J.G., Li, W., 2021. Study on CO₂ foam fracturing model and fracture propagation simulation. Energy, 121778. https://doi.org/10.1016/j.energy.2021.121778.

Dehghan, A.N., Goshtasbi, K., Ahangari, K., Jin, Y., Bahmani, A., 2017. 3D numerical modeling of the propagation of hydraulic fracture at its intersection with

natural (pre-existing) fracture. Rock Mech. Rock Eng. 50 (2), 367–386. https://doi.org/10.1007/s00603-016-1097-7.

- Fan, T.G., Xu, X.F., Fan, L., Feng, Y.Q., Liu, W.H., Liu, J.T., Wang, M.Y., Jia, G.Q., 2021. Geological characteristics and exploration prospect of shale oil in permian lucaogou formation, santanghu basin. China Petroleum Exploration, 2021 26 (4), 125–136. https://doi.org/10.3969/j.issn.1672-7703.2021.04.010.
- Fries, T., Baydoun, M., 2012. Crack propagation with the extended finite element method and a hybrid explicit—implicit crack description. Int. J. Numer. Methods Eng. 89 (12), 1527—1558. https://doi.org/10.1002/nme.3299.
- Gale, J.F.W., Laubach, S.E., Olson, J.E., Eichhubl, P., Fall, A., 2014. Natural fractures in shale: a review and new observations. AAPG Bull. 98 (11), 2165–2216. https://doi.org/10.1306/08121413151.
- Gale, J.F.W., Reed, R.M., Holder, J., 2007. Natural fractures in the Barnett shale and their importance for hydraulic fracture treatments. AAPG Bull. 91 (4), 603–622. https://doi.org/10.1306/11010606061.
- Grieser, W.V., Bray, J.M., 2007. Identification of production potential in unconventional reservoirs. In: Production and Operations Symposium. Society of Petroleum Engineers. https://doi.org/10.2523/106623-MS.
- Gu, H., Weng, X., 2010. Criterion for fractures crossing frictional interfaces at non-orthogonal angles. In: The 44th U.S. Rock Mechanics Symposium and 5th U.S.-Canada Rock Mechanics Symposium. ARMA 10-198.
- Guo, T., Tang, S., Liu, S., Xu, J., Qi, N., Rui, Z., 2020. Physical simulation of hydraulic fracturing of large-sized tight sandstone outcrops. SPE J. 26 (01), 372–393. https://doi.org/10.2118/204210-PA.
- Han, S.B., Hu, X.D., Zhou, F.J., Qiu, Y., Li, M.H., Huang, G.P., 2021. Influence of temperature on the interaction of metal veins and hydraulic fractures in shale formations: experiment and simulation. J. Petrol. Sci. Eng. 200, 108372. https://doi.org/10.1016/j.petrol.2021.108372.
- He, Y., Cheng, S., Sun, Z., Chai, Z., Rui, Z., 2020. Improving oil recovery through fracture injection and production of multiple fractured horizontal wells. J. Energy Resour. Technol. 142 (5), 053002. https://doi.org/10.1115/1.4045957.
- Jiang, Y.L., Lian, H.J., Nguyen, V.P., Liang, W.G., 2019. Propagation behavior of hydraulic fracture across the coal-rock interface under different interfacial friction coefficients and a new prediction model. J. Nat. Gas Sci. Eng. 68, 102894. https://doi.org/10.1016/j.jngse.2019.05.07.
- Kolawole, O., Ispas, I., 2019. How hydraulic fractures interact with natural fractures: a review and new observations. In: The 53rd U.S. Rock Mechanics/Geomechanics Symposium. New York City, New York, June 2019. ARMA 19–018.
- Kuruppu, M.D., Obara, Y., Ayatollahi, M.R., Chong, K.P., Funatsu, T., 2014. The ISRM-suggested method for determining the mode I static fracture toughness using semi-circular bend specimen. Rock Mechanics and Rock Engineering 267–274. https://doi.org/10.1007/978-3-319-07713-0.
- Lecampion, B., 2009. An extended finite element method for hydraulic fracture problems. Commun. Numer. Methods Eng. 25 (2), 121–133. https://doi.org/
- Lee, H.P., Olson, J.E., Holder, J., Gale, J.F.W., Myers, R.D., 2015. The interaction of propagating opening mode fractures with preexisting discontinuities in shale. Geophys. Res. Solid Earth 169–181. https://doi.org/10.1002/2014jb011358.
- Lee, H.P., Olson, J.E., Schultz, R.A., 2018a. Interaction analysis of propagating opening mode fractures with veins using the discrete element method. Int. J. Rock Mech. Min. Sci. 103, 275–288. https://doi.org/10.1016/j.ijrmms.2018.01.005.
- Lee, H.P., Razavi, O., Olson, J.E., 2018b. Hydraulic fracture interaction with cemented natural fracture: a three dimensional discrete element method analysis. SPE Hydraulic Fracturing Technology Conference and Exhibition. https://doi.org/ 10.2118/189852-ms.
- Lee, H.P., Olson, J.E., Schultz, R.A., 2016. The interaction analysis of propagating opening mode fractures with veins using discrete element method. ARMA 16-769. https://doi.org/10.1016/j.ijrmms.2018.01.005.
- Lim, I.L., Johnson, I.W., Choi, S.K., 1993. Stress intensity factors for semi-circular specimens under three-point bending. Eng. Fract. Mech. 44 (3), 363–382. https://doi.org/10.1016/0013-7944(93)90030-v.
- Lim, I.L., Johnston, I.W., Choi, S.K., Boland, J.N., 1994. Fracture testing of a soft rock

- with semi-circular specimens under three-point bending. Part 1-Mode I. Int. J. Fract, 31 (3), 199–212. https://doi.org/10.1016/0148-9062(94)90463-4.
- Li, M., Zhou, F., Yuan, L., et al., 2021. Numerical modeling of multiple fractures competition propagation in the heterogeneous layered formation. Energy Rep. 7, 3737—3749. https://doi.org/10.1016/j.egyr.2021.06.061.
- Li, M., Lv, W., Liu, J., et al., 2022a. Effect of perforation friction on 3D In-stage multiple fracture propagation: a numerical study. Eng. Fract. Mech. 267, 108415. https://doi.org/10.1016/j.engfracmech.2022.108415.
- Li, M., Zhou, F., Liu, J., et al., 2022b. Quantitative investigation of multi-fracture morphology during TPDF through true tri-axial fracturing experiments and CT scanning. Petrol. Sci. 19 (4), 1700–1717. https://doi.org/10.1016/ i.petsci.2022.03.017.
- Li, M., Zhou, F., Sun, Z., et al., 2022c. Experimental study on plugging performance and diverted fracture geometry during different temporary plugging and diverting fracturing in Jimusar shale. J. Petrol. Sci. Eng. 110580. https://doi.org/ 10.1016/j.petrol.2022.110580.
- Li, Y.W., Jia, D., Rui, Z.H., Peng, J.Y., Fu, C.K., Zhang, J., 2017. Evaluation method of rock brittleness based on statistical constitutive relations for rock damage. J. Petrol. Sci. Eng. 153, 123–132. https://doi.org/10.1016/j.petrol.2017.03.041.
- Li, Y.W., Long, M., Tang, J.Z., Chen, M., Fu, X.F., 2020. A hydraulic fracture height mathematical model considering the influence of plastic region at fracture tip. Petrol. Explor. Dev. 47, 184–195. https://doi.org/10.1016/s1876-3804(20)60017-9.
- Pan, R., Zhang, G.Q., Xing, Y.K., Li, S.Y., Zheng, X.L., Tang, M.R., 2019. The experimental study of the shale bedding impact on fracture energy anisotropy. The 53rd U.S. Rock Mechanics/Geomechanics Symposium. ARMA 19–96.
- Renshaw, C.E., Pollard, D.D., 1995. An experimentally verified criterion for propagation across unbounded frictional interfaces in brittle, linear elastic materials. Int. J. Rock Mech. Min. Sci. Geomech. Abstr. 32 (3), 237–249. https://doi.org/10.1016/0148-9062/96\ightarrow83899-x.
- Rui, Z., Guo, T., Feng, Q., Qu, Z., Qi, N., Gong, F., 2018. Influence of Gravel on the propagation pattern of hydraulic fracture in the Glutenite Reservoir. J. Petrol. Sci. Eng. 165, 627–639. https://doi.org/10.1016/j.petrol.2018.02.067.
- Stolarska, M., Chopp, D., Moës, N., Belytschko, T., 2001. Modelling crack growth by level sets in the extended finite element method. Int. J. Numer. Methods Eng. 51, 943–960. https://doi.org/10.1002/nme.201.
- Virgo, S., Abe, S., Urai, J.L., 2013. Extension fracture propagation in rocks with veins: insight into the crack-seal process using Discrete Element Method modeling. J. Geophys. Res. Solid Earth 118 (10), 5236–5251. https://doi.org/10.1002/2013jb010540.
- Wang, B., Zhou, F.J., Wang, D.B., Liang, T.B., Yuan, L.S., Hu, J., 2018. Numerical simulation on near-wellbore temporary plugging and diverting during refracturing using XFEM-Based CZM. J. Nat. Gas Sci. Eng. 55, 368—381. https://doi.org/10.1016/j.jngse.2018.05.009.
- Wang, W.W., Olson, J.E., Prodanovic, M., Schultz, R.A., 2018. Interaction between cemented natural fractures and hydraulic fractures assessed by experiments and numerical simulations. J. Petrol. Sci. Eng. 167, 506–516. https://doi.org/ 10.1016/j.petrol.2018.03.095.
- Wang, W.W., Olson, J.E., Prodanović, M., 2013. Natural and hydraulic fracture interaction study based on semi-circular bending experiments. SPE/AAPG/SEG Unconventional Resources Technology Conference. https://doi.org/10.1190/ urtec2013-168.
- Xu, L., Chang, Q.S., Yang, C.K., Tao, Q.E., Wang, S.L., Fei, L.Y., Xu, S.L., 2019. Characteristics and oil-bearing capability of shale oil reservoir in the Permian Lucaogou Formation. Jimusaer sag. Oil & Gas Geology, 2019 40 (3), 535–549. https://doi.org/10.11743/ogg20190309.
- Yang, H., Chen, S., Xie, Y., Yang, C., 2020. Shale reservoir characteristics and their influencing factors in the Lucaogou Formation, southeastern margin of the Junggar Basin, China. Geophysical Prospecting for Petroleum. 2020 59 (4), 583–595. https://doi.org/10.3969/ji.ssn.1000G1441.2020.04.009 (in Chinese).
- Zeng, Q.D., Liu, W.Z., Yao, J., 2018. Numerical modeling of multiple fractures propagation in anisotropic formation. J. Nat. Gas Sci. Eng. 53, 337–346. https://doi.org/10.1016/j.jngse.2018.02.035.